Magnetic field effect on Higgs boson production rate through gluon fusion

Jorge Jaber-Urquiza

Facultad de Ciencias, UNAM

36th Annual Hampton University Graduate Studies
e-HUGS 2021

June 17, 2021

Why is Higgs boson so important?

- Higgs field is responsible for generating the masses of the elementary particles of the Standard Model (SM).

- This occurs through the spontaneous breaking of the electroweak symmetry.

- Since the confirmation of its existence in 2012, studying its properties became the main objective of the Higgs physics program.

- Precisely characterizing the properties of the Higgs boson would help us better understand the nature of spontaneous breaking of electroweak symmetry.[1], Yukawa's couplings[2], etc.

---

[1] M. Bier *et al.* *JHEP* **01**, 164, (2014).
[2] A. M. Sirunyan *et al.* *Phys. Lett.* B **778**, 101, (2018).

External agents

- So far, all the research referred has focused only on the physics of the Higgs boson in vacuum (proton-proton collisions).

- Nevertheless, they can be extended to scenarios where the effects of external agents could change the global properties of the Higgs boson.[3]

- It is important to quantify the effect of these external agents in perturbative calculations to have clarity on the effects caused by "new physics".

---

[3] G. Gamow. *Phys. Rev.* **70**, 572, (1946).

New scenarios for Higgs physics

Recent studies show the possibility of quark-gluon plasma (QGP) being produced in nucleon-nucleon collisions[4,5]

Possible Formation of QGP-droplets in Proton-Proton Collisions at the CERN Large Hadron Collider

RAGHUNATH SAHOO*
DISCIPLINE OF PHYSICS, SCHOOL OF BASIC SCIENCES,
INDIAN INSTITUTE OF TECHNOLOGY INDORE, SIMROL, KHANDWA ROAD, INDORE-453552, INDIA

ABSTRACT

Proton-proton (pp) collisions have been traditionally used as a baseline measurement in the search for a deconfined state of matter in heavy-ion collisions at ultra-relativistic energies. The unprecedented collision energies that are available at the Large Hadron Collider (LHC) at the European Laboratory for Nuclear Research (CERN) have illuminated new challenges in understanding the possible formation of droplets of this deconfined matter of partonic degrees of freedom in hadronic col-

========= **FIELDS, PARTICLES,** =========
AND NUCLEI
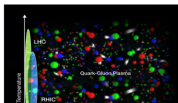
Onset of the Jet Quenching Phenomenon

M. T. AlFiky[a, *], O. Elsherif[b, **], and A. M. Hamed[a, c, ***]

[a] Department of Physics, The American University in Cairo, New Cairo, 11835 Egypt
[b] Department of Physics and Astronomy, Texas A&M University, College Station, 77843 TX, USA
[c] Department of Physics and Astronomy, University of Mississippi, Oxford, 38677 MS, USA
*e-mail: alfiky@aucegypt.edu
**e-mail: martam@buffalo.edu
***e-mail: ahamed@comp.tamu.edu
Received November 2, 2019, revised November 16, 2019, accepted November 17, 2019

The aim of this study is to set a baseline for the jet quenching measurements of the Quark Gluon Plasma formed in the large system size Nucleus–Nucleus (A–A) at top central collisions, via studying simulated small system size, Nucleon–Nucleon (N–N) collisions. The proton–proton (p–p) collisions are being simulated using PYTHIA, at center of mass energies $\sqrt{s_{NN}}$ = 200 GeV and $\sqrt{s_{NN}}$ = 13 TeV corresponding to the available energies at the current collider experiments; the Relativistic Heavy Ion Collider, and the Large Hadron Collider. At both energies, the two-particle azimuthal correlation functions have been considered, and the yield associated with the high transverse momentum (p_T) particles are extracted at its near-side ($\Delta\phi \approx 0$) and away-side ($\Delta\phi = \pi$) at mid pseudo-rapidity ($|\eta| \leq 2$). The ratio between the near-side yields in the high multiplicity events to these of the low multiplicity events (I_{NS}^{T}), as well as, the ratio of the away-side yields (I_{AS}^{T}) were calculated as a function of the hadron fractional energy z_T of the high-p_T particle. At both energies, the values of I_{NS}^{T} and I_{AS}^{T} were found to be close to unity, and of trivial dependence on z_T. The values of I_{AS}^{T} are always less than these of I_{NS}^{T} at the same multiplicity and energy, and both quantities show a pattern of systematic decreases with the multiplicity. Such multiplicity dependence cannot be used neither to exclude the jet quenching nor to prove it in the high multiplicity events in p–p collisions, as the suppressions have been found at both sides, near and away of the high-p_T particle.

─────────
[4] AAPPS Bull. **29**, 16-21, (2019).
[5] JETP Letters **111**, 8-17, (2020).

There is also the possibility of the detection of Higgs bosons in other types of collisions; for example, in relativistic heavy ion collisions[6],[7]

Production and Hadronic Decays of Higgs Bosons in Heavy-Ion Collisions

Edmond L. Berger,[1,*] Jun Gao,[2,1] Adil Jueid,[2,3] and Hao Zhang[3,4,§]
[1]High Energy Physics Division, Argonne National Laboratory, Argonne, Illinois 60439, USA
[2]INPAC, Shanghai Key Laboratory for Particle Physics and Cosmology, School of Physics and Astronomy, Shanghai Jiao Tong University, Shanghai 200240, China
[3]Theoretical Physics Division, Institute of High Energy Physics, Chinese Academy of Science, Beijing 100049, China
[4]School of Physics, University of Chinese Academy of Science, Beijing 100049, China

We examine Higgs boson production and decay in heavy-ion collisions at the LHC and future colliders. Owing to the long lifetime of the Higgs boson, its hadronic decays may experience little or no screening from the hot and dense quark-gluon plasma, whereas jets from hard scattering processes and from decays of the electroweak gauge bosons and the top quark suffer significant energy loss. This distinction can lead to enhanced signal to background ratios in hadronic decay channels and thus, for example, provide alternative ways to probe the Yukawa coupling of the Higgs boson to the bottom quark and its lifetime.

Introduction.—The successful operation of the CERN Large Hadron Collider (LHC) led to the discovery of the Higgs boson, the final piece of the standard model (SM) [1,2] of particle physics. Precise measurements of the properties and couplings of the Higgs boson are now

(EW) gauge bosons and the top quark, this timescale is shorter than the lifetime of the Higgs boson (which is ~47 fm/c). The consequences include the following. (i) Particles from Higgs decay, which do not travel in the QGP, will carry information on the Higgs boson. (ii) Because

Higgs boson production in photon-photon interactions with proton, light-ion, and heavy-ion beams at current and future colliders

David d'Enterria[*]
CERN, European Organization for Nuclear Research, 1211 Geneva, Switzerland

Daniel E. Martins[†]
UFRJ, Univ. Federal do Rio de Janeiro, 21941-901 Rio de Janeiro, RJ, Brazil

Patricia Rebello Teles[‡]
UERJ, Univ. do Estado do Rio de Janeiro, 20550-900 Rio de Janeiro, RJ, Brazil

The production of the Higgs boson in photon-photon interactions with proton and nuclous beams at three planned or proposed future CERN colliders—the high-luminosity Large Hadron Collider (HL-LHC), the high-energy LHC (HE-LHC), and the Future Circular Collider (FCC)—is studied. The cross sections for the process $AA \overset{\gamma\gamma}{\to} A(H(A)$, with the ions A surviving the interaction and the Higgs scalar exclusively produced, are computed with MADGRAPH 5 modified to include the corresponding elastic γ fluxes, for Pb-Pb, Xe-Xe, Kr-Kr, Ar-Ar, O-O, p-Pb, and p-p over the nucleon-nucleon center energy range $\sqrt{s_{NN}} \approx 3$–100 TeV. Simulations of the $\gamma\gamma \to H \to b\bar{b}$ decay mode—including realistic (mis)tagging and reconstruction efficiencies for the final-state b-jets, as well as appropriate kinematical selection criteria to reduce the similarly computed $\gamma\gamma \to b\bar{b}$, $c\bar{c}$, $q\bar{q}$ continuum backgrounds—have been carried out. Taking into account the expected luminosities for all systems, the yields, and significances for observing the Higgs boson in ultraperipheral collisions (UPCs) are estimated. At the HL-LHC and HE-LHC, the colliding systems with larger Higgs significance are Ar-Ar (6.3 TeV) and Kr-Kr (12.5 TeV), respectively, but 3σ evidence for two-photon Higgs production would require 200 and 30 times larger integrated luminosities than those planned today at both machines. Factors of 10 can be gained by running for a year, rather than

----
[6]Phys. Rev. Lett. **122**, 041803, (2019).
[7]Phys. Rev. D **101**, 033009, (2020).

Magnetic fields in relativistic heavy ion collisions

- Very intense in early stages[8], $eB \sim m_\pi^2$.
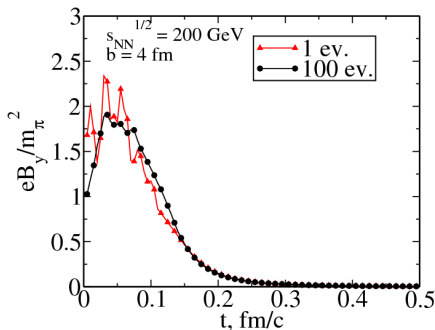
- Decrease exponentially, $\tau \sim$ fm/c.

Figure: The time evolution of the magnetic field strength eB_y at the central point O in Au-Au collisions with impact parameter $b = 4$fm in the UrQMD model, in one event ("1ev") and and averaged over 100 events ("100ev"). The symbols are plotted every $\Delta t = 0.2$fm/c for $E_{\text{lab}} = 60$GeV and $\Delta t = 0.01$fm/c for $\sqrt{S_{NN}} = 200$GeV.

[8] V. V. Skokov *et al.* *Nucl. Phys.* A **24**, 708, (2009).

Higgs production through gluon fusion

The production of Higgs bosons through gluon fusion is a highly relevant process because it corresponds to more than 90% of the cross section at 13 TeV[9]

$$gg \longrightarrow H.$$

This process has the following probability amplitude associated

$$\langle p_3; + \big| (p_1, \mu, \sigma, a), (p_2, \nu, \sigma', b); - \rangle. \tag{1}$$

At leading order there are two different contributions to the amplitude, i.e. two Feynman diagrams.

---

[9]M. Tanabashi *et al.* Phys. Rev. D **98**, 03001, (2018).
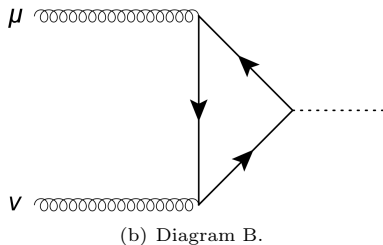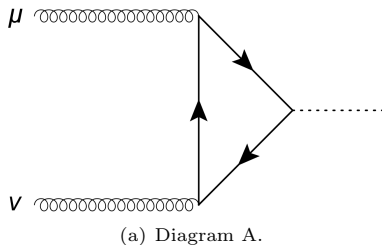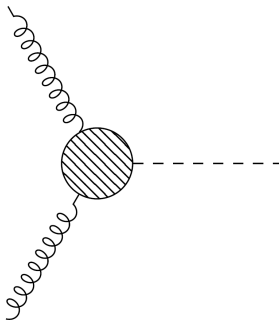
(a) Diagram A.

(b) Diagram B.

Figure: Feynman diagrams of Higgs production through gluon fusion at LO.

Effective vertex

These two diagrams could be seen as an "effective vertex" $\Gamma^{\mu\nu}$, where all the information of the Higgs production process through gluon fusion is contained. The effective vertex represents a direct coupling between the Higgs and the gluons.
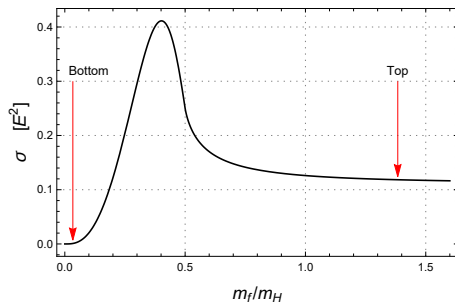
Cross section

The unpolarized cross section is

$$\sigma = \frac{1}{2m_H^2} 2\pi\delta\left(\mathcal{S} - m_H^2\right) \overline{\sum}_{\text{color,spin}} |\mathcal{M}|^2, \tag{2}$$
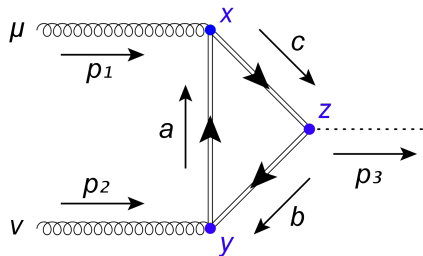
with

$$i\mathcal{M} = i\Gamma^{\mu\nu}(p_1, p_2)\epsilon_\mu^a(p_1, \sigma)\epsilon_\nu^b(p_2, \sigma'). \tag{3}$$
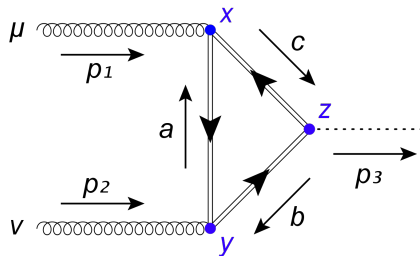
Higgs boson production through gluon fusion in presence of an external magnetic field

The two different Feynman diagrams in Fig.2 are

(a) Diagram A.

(b) Diagram B.

Figure: Feynman diagrams at leading order process in the presence of an external magnetic field. The magnetic field is represented by a double line in the fermionic propagators.

The fermionic propagator in the presence of a magnetic field was obtained by Schwinger (in the configuration space) and is given by[10]

$$S_F^B(x,y) = \Omega(x,y) \int \frac{d^4p}{(2\pi)^4} S_F^B(p) e^{-ip\cdot(x-y)}, \tag{4}$$

where

$$\Omega(x',x'') = \exp\left(-iq \int_{x''}^{x'} A_\mu(x) dx^\mu\right) \tag{5}$$

it's known as Schwinger phase, with q the electric charge of the fermion and A_μ the potential that generates the magnetic field B.

---

[10]A. Erdas. *Phys. Rev.* D **82**, 664, (2009).

If the magnetic field defines the z direction, the invariant part of the propagator is[11]

$$
\begin{aligned}
S_f^B(p) = \int_0^\infty \frac{ds}{\cos(qBs)} \exp\Bigg[&-is\left(m_f^2 - p_\parallel^2 - p_\perp^2 \frac{\tan(qBs)}{qBs}\right)\Bigg] \\
&\times \left[\left(m_f + \slashed{p}_\parallel\right) e^{-iqBs\Sigma_3} + \frac{\slashed{p}_\perp}{\cos(qBs)}\right],
\end{aligned}
\tag{6}
$$

where $p_\parallel$ and $p_\perp$ are the parallel and perpendicular components of the momentum to the magnetic field and

$$
\Sigma_3 = i\gamma^1\gamma^2.
\tag{7}
$$

[11] A. Erdas. *Phys. Rev.* D **82**, 664, (2009).

Applying Feynman's rules to diagram A gives

$$
\begin{aligned}
i\Gamma_{qB\,(A)}^{\;\;\mu\nu}(x,y,z) &= -\mathcal{TR}\left[(-ig_s\gamma^\mu t^a)S_f^{q_B}(x,y)(-ig_s\gamma^\nu t^b)S_f^{q_B}(y,z)(-ig_f)S_f^{q_B}(z,x)\right] \\
&= -ig_s^2 g_f \,\mathbf{tr}\left[t^a t^b\right]\Omega_q(x,y)\Omega_q(y,z)\Omega_q(z,x) \\
&\quad \times \int \frac{d^4a}{(2\pi)^4}\frac{d^4b}{(2\pi)^4}\frac{d^4c}{(2\pi)^4}e^{-ia\cdot(x-y)}e^{-ib\cdot(y-z)}e^{-ic\cdot(z-x)} \\
&\quad\quad\quad\quad \times Tr\left[\gamma^\mu S_f^{q_B}(a)\gamma^\nu S_f^{q_B}(b)S_f^{q_B}(c)\right].
\end{aligned}
\tag{8}
$$

And to diagram B

$$
\begin{aligned}
i\Gamma_{qB\,(B)}^{\;\;\mu\nu}(x,y,z) &= -ig_s^2 g_f \,\mathbf{tr}\left[t^a t^b\right]\Omega_q(z,y)\Omega_q(x,z)\Omega_q(y,x) \\
&\quad \times \int \frac{d^4a}{(2\pi)^4}\frac{d^4b}{(2\pi)^4}\frac{d^4c}{(2\pi)^4}e^{-ia\cdot(x-y)}e^{-ib\cdot(y-z)}e^{-ic\cdot(z-x)} \\
&\quad\quad\quad\quad \times Tr\left[\gamma^\nu S_f^{q_B}(-a)\gamma^\mu S_f^{q_B}(-c)S_f^{q_B}(-b)\right].
\end{aligned}
\tag{9}
$$

Working out a little bit we arrive at

$$
i\Gamma^{\mu\nu}_{qB\,(A/B)}(p_1,p_2) = -ig_s^2 g_f \,\mathbf{tr}\left[t^a t^b\right]\left(\frac{4\pi}{qB}\right)^{d-2}
$$
$$
\times \int_0^\infty \frac{ds_1 ds_2 ds_3}{\cos(qBs_1)\cos(qBs_2)\cos(qBs_3)} G_{(A/B)}\tilde{T}^{\mu\nu}_{(A/B)},
$$

(10)

with

$$
G_{(A/B)} = \frac{2^{4-3d}}{s\pi^{\frac{3d}{2}-2}}\left(\frac{-iqB\cos(s_1)\cos(s_1+s_2)}{\sin(s)}\right)^{\frac{d}{2}-1}\left(\frac{(qB)^2\cot(s_3)}{\cot(s_3)-\tan(s_2)}\right)^{\frac{d}{2}-1}
$$
$$
\times e^{\frac{i}{qB}\frac{\cos(s_1)\cos(s_2)\sin(s_3)}{\sin(s)}\left[\tan(s_1)\left(\tan(s_2)\cot(s_3)p_{2_\perp}^2+p_{1_\perp}^2\right)+\tan(s_2)(p_1+p_2)_\perp^2\right]}
$$
$$
\times e^{-ism_f^2}e^{\frac{i}{s}\left((s_1+s_2)s_3 p_{1_\parallel}^2+(s_1+s_3)s_2 p_{2_\parallel}^2+2s_2 s_3(p_1\cdot p_2)_\parallel\right)}
$$
$$
\times e^{\mp\frac{2i}{qB}\frac{\cos(s_1)\cos(s_2)\sin(s_3)}{\sin(s)}\tan(s_1)\tan(s_2)p_1\hat{F}p_2}.
$$

(11)

Approximations

The integrals that remain to be solved over the s_i parameters cannot be calculated analytically, so it is necessary to carry out certain approximations.

The most frequently used approaches in the literature are

- Weak magnetic field.

- Strong magnetic field.

These approximations are taken when $qB \ll m_f^2$ y $qB \gg m_f^2$, respectively[12].

_____

[12]To get a reference, the critical magnetic field for a electron is 4.4×10^{13}G $\sim (0.5 MeV)^2$
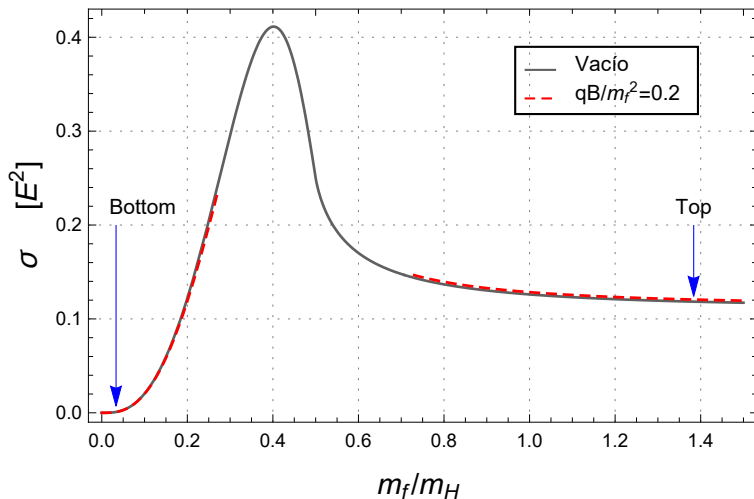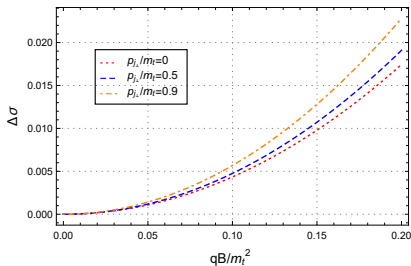
Figure: Behavior of the partial cross section as a function of the mass of the quarks within the fermionic loop, taking $\Theta = \pi$, $p_{i_\perp} = 0.5 m_f$ and $qB = 0.2 m_f^2$.
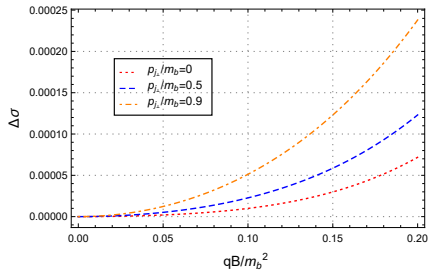
Magnetic field effects

To quantify more precisely the effect of both the magnetic field and the transverse moment of gluons, it is convenient to define

$$\Delta\sigma \equiv \frac{\sigma_{LO, \text{ partial}}^{qB} - \sigma_{LO, \text{ vacuum}}}{\sigma_{LO, \text{ vacuum}}}. \tag{12}$$
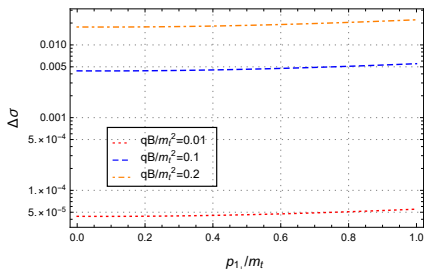
(a) Top quark.

(b) Bottom quark.

Figure: Behavior of the response of the effective section as a function of the magnetic field for the top and bottom quarks, taking different values of the transverse moment and $\Theta = \pi$.
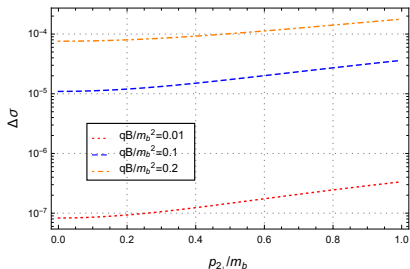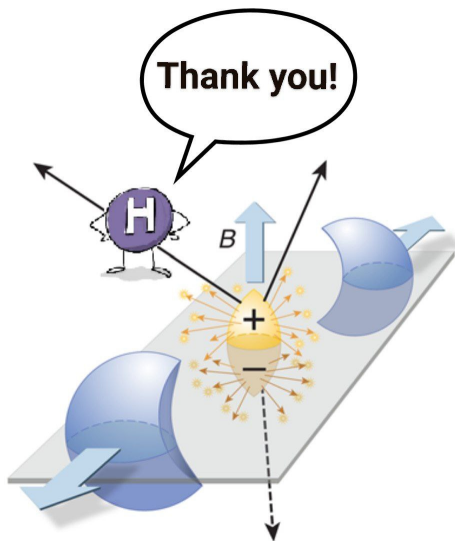
(a) Top quark.

(b) Bottom quark.

Figure: Behavior of the response of the effective section as a function of $p_{i_\perp}$ for the top and bottom quarks taking different values for the magnetic field, $p_{j_\perp} = 0.2 m_f$ y $\Theta = \pi$.

What's next?

- Calculate the total cross section in the presence of magnetic field.

- Take an approximation that allows studying an arbitrary interval for the magnitudes of the transverse components of the moment.

- For light quarks you must work with a strong field approximation.

- A more complete analysis should include the effects of temperature.

- Electroweak corrections.

Beyond Standard Model?

- Measurements of the properties of the Higgs boson open a new window for understanding fundamental interactions and for exploring possible extensions to the laws of physics that we know.

- If small deviations can be found between the theoretical predictions and the experimental data, these could be a sign of new physics, physics beyond the Standard Model (BSM).

- A precision physics program, both theoretical and experimental, of the properties of the Higgs boson would be of great relevance as it could provide evidence, directly or indirectly, of BSM physics.

- LHC has entered a stage where precision measurements of Higgs properties play a central role.

Higgs production through gluon fusion

- The contribution to this process due to pure QCD interactions is around 95% while QCD-electroweak (QCD-EW) interactions contribute approximately 5%[13].

- "Leading-order" (LO) [14]

- "Next-to-leading-order" (NLO) $\sim 80 - 100\%$[15]

- "Next-to-next-to-leading-order" (NNLO or N^{2}LO) $\sim 10 - 20\%$[16]

- "Next-to-next-to-next-to-leading order" (N^{3}LO) $\sim 4 - 6\%$[17]

---

[13] M. Tanabashi *et al.* Phys. Rev. D **98**, 03001, (2018).

[14] H. M. Georgi *et al.* Phys. Rev. Lett. **40**, 692, (1978).

[15] M. Spira *et al.* Phys. Lett. B **453**, 17, (1995).

[16] C. Anastasious. *Nucl. Phys.* B **646**, 220, (2002).

[17] C. Anastasious *et al.* *JHEP* **05**, 058, (2016).

Relativistic heavy ion collisions

In relativistic heavy ion collisions, it is possible to create an extreme high temperature and density environment that evolves over time[18]

- t=0 fm/c: In this initial stage the hadronic jets, direct photons, pairs of dileptons, heavy quarks, and vector bosons are produced.

- t∼0.2 fm/c: A state called "glasma" is created, it's made up of non-equilibrium partonic matter at high density[19].

- t∼1 fm/c: The partons that make up the "glasma" begin to interact strongly (QCD) with each other and a thermal equilibrium is reached.

- The result of this thermalization is a phase of QCD at high temperature known as "quark-gluon plasma" (QGP).

---

[18]E. Iancu. arXiv:1205.0579 [hep-ph].

[19]T. Lappi *et al. Nucl. Phys.* **A 772**, 200, (2006).

Quark-gluon plasma

- The characteristic time for the expansion and cooling of the QGP is of the order of 10 fm/c[20].

- The mean lifetime of the Higgs boson is $\tau \sim 47$ fm/c[21].

- Taking this in consideration, we could imagine the following physical situations:

  - A Higgs boson produced in the initial stage of the collision (before the formation of the QGP) is affected by the plasma and modifies some of its properties such as the lifetime, the kinematic distribution, the decay rate, etc.

  - A Higgs boson is produced within the QGP, so that the main effect of the thermalized medium will be observed in the production rate.

---

[20] R. Shen *et al.* *Phys. Rev.* C **86**, 049903(E), (2012)

[21] M. Tanabashi *et al.* Phys. Rev. D **98**, 03001, (2018).

What else?

The Higgs field is described by a neutral scalar field, so the results of this research can be generalized and applied to various physical processes where a scalar field plays a central role.

- Inflation[22].

- Compact astrophysical objects (color superfluidity[23]).

- Production of different (pseudo)scalar particles in relativistic heavy ion collisions such as mesons (π, B, D), etc.

---

[22] T. Matos *et al.* *Classical Quantum Gravity* **17**, 1707, (2000)

[23] M. Alford *et al.* *Phys. Lett.* B **422**, 247, (1998).

Feynman rules

- Propagator

$$j, f \xrightarrow{\quad p \quad} k, f' = \frac{i\delta_k^j \delta_{f'}^f}{\not{p} - m_f + i\epsilon}.$$

- Vertices

(a) Yukawa.

$$= -ig_f \delta_k^j \delta_{f'}^f.$$

(b) Gluon-quark.

$$= -ig_s \gamma^\mu (t^a)^j{}_k \delta_{f'}^f.$$

Figure: Interaction vertices.

How does it looks the vertex?

Taking into account the tensor structures that are available in this process[24]

$$\text{Vacuum: } p_1^\mu, \, p_2^\mu, \, g^{\mu\nu} \, \& \, \epsilon^{\mu\nu\alpha\beta}.$$

$$\text{Magnetic field: } \quad F^{\mu\nu}, \, F^{*\mu\nu} \, \& \, F^\mu{}_\alpha F^{\alpha\nu}.$$

In the magnetic field case there are more than 60 different rank-two tensors available for the vertex. The most general form includes them all!

Good news, the effective vertex must be such that it fulfills certain properties and it simplifies a little bit its tensor structure.

---

[24] I. Batalin and A. Shabad. *Zh. Eksp. Teor. Fiz.* **60**, 894, (1971).

- Slavnov-Taylor identities

$$p_1^\mu \Gamma_{\mu\nu}(p_1, p_2) = 0, \tag{13}$$
$$p_2^\nu \Gamma_{\mu\nu}(p_1, p_2) = 0. \tag{14}$$

- Boson symmetry

$$\Gamma^{\mu\nu}(p_1, p_2) = \Gamma^{\nu\mu}(p_2, p_1). \tag{15}$$

Taking into account this proprieties and the gluons on-shell, the tensor structure that the effective vertex must take is

$$\Gamma_{qB}^{\mu\nu}(p_1, p_2) = A \left[g^{\mu\nu} - \frac{p_1^\nu p_2^\mu}{p_1 \cdot p_2} \right] + B \frac{p_1^\mu p_2^\nu}{p_1 \cdot p_2} + C \frac{\hat{F}^\mu p_1 \hat{F}^\nu p_2}{p_1 \cdot p_2}$$
$$+ D \left[g_\perp^{\mu\nu} - \frac{p_{1\perp}^\nu p_{2\perp}^\mu}{(p_1 \cdot p_2)_\perp} \right] + 9 \text{ more terms.} \tag{16}$$

Tensor structure in a magnetic field

$$
\begin{aligned}
\Gamma_{qB}^{\mu\nu}(p_1,p_2) =& A\left[g^{\mu\nu} - \frac{p_1^\nu p_2^\mu}{p_1\cdot p_2}\right] + B\frac{p_1^\mu p_2^\nu}{p_1\cdot p_2} + C\frac{\hat{F}^\mu p_1 \hat{F}^\nu p_2}{p_1\cdot p_2} + D\left[g_\perp^{\mu\nu} - \frac{p_{1_\perp}^\nu p_{2_\perp}^\mu}{(p_1\cdot p_2)_\perp}\right] \\
&+ E\left[\frac{p_1^\mu p_1^\nu + p_2^\mu p_2^\nu}{p_1\cdot p_2} - \frac{p_1^\mu p_{1_\perp}^\nu + p_2^\nu p_{2_\perp}^\mu}{(p_1\cdot p_2)_\perp}\right] + G\left[g^{\mu\nu} + \frac{(p_1\cdot p_2)g_\perp^{\mu\nu} - p_1^\nu p_{2_\perp}^\mu - p_2^\mu p_{1_\perp}^\nu}{(p_1\cdot p_2)_\perp}\right] \\
&+ H\left(p_2\hat{F}p_1\right)\left[g^{\mu\nu}\frac{p_2\hat{F}p_1}{(p_1\cdot p_2)^2} - \frac{(p_1\cdot p_2)\hat{F}^{\mu\nu} + p_2^\mu \hat{F}^\nu p_1 - p_1^\nu \hat{F}^\mu p_2}{(p_1\cdot p_2)^2}\right] \\
&+ I\left[\left(p_2\hat{F}p_1\right)^2\frac{p_1^\mu p_1^\nu + p_2^\mu p_2^\nu}{(p_1\cdot p_2)^3} - \left(p_2\hat{F}p_1\right)\frac{p_1^\mu \hat{F}^\nu p_1 - p_2^\nu \hat{F}^\mu p_2}{(p_1\cdot p_2)^2}\right] \\
&+ J\left[\hat{F}^{\mu\nu}\frac{p_2\hat{F}p_1}{p_1\cdot p_2} - \frac{\hat{F}^\mu p_2 \hat{F}^\nu p_1}{p_1\cdot p_2}\right] + K\left(p_2\hat{F}p_1\right)\frac{p_1^\mu \hat{F}^\nu p_2 - p_2^\nu \hat{F}^\mu p_1}{p_1\cdot p_2} \\
&+ L\left[\frac{\hat{F}^\mu p_1 \hat{F}^\nu p_1 + \hat{F}^\mu p_2 \hat{F}^\nu p_2}{p_1\cdot p_2} - \left(p_2\hat{F}p_1\right)\frac{p_1^\nu \hat{F}^\mu p_1 - p_2^\mu \hat{F}^\nu p_2}{(p_1\cdot p_2)^2}\right] \\
&+ M\left(p_2\hat{F}p_1\right)\left[g_\perp^{\mu\nu}\frac{p_2\hat{F}p_1}{(p_1\cdot p_2)^2} - (p_1\cdot p_2)_\perp\frac{\hat{F}^{\mu\nu} + p_{2_\perp}^\mu \hat{F}^\nu p_1 - p_{1_\perp}^\nu \hat{F}^\mu p_2}{(p_1\cdot p_2)^2}\right] \\
&+ N\left(p_2\hat{F}p_1\right)\left[\frac{p_{1_\perp}^\nu \hat{F}^\mu p_1 - p_{2_\perp}^\mu \hat{F}^\nu p_2}{(p_1\cdot p_2)^2} + (p_1\cdot p_2)_\perp\frac{p_2^\mu \hat{F}^\nu p_2 - p_1^\nu \hat{F}^\mu p_1}{(p_1\cdot p_2)^3}\right].
\end{aligned}
$$

Taking the Fourier transform of the effective vertex it's possible to identify easily Dirac deltas in the parallel coordinates but not in the perpendicular ones due to the phase that the diagram has acquired. Carrying out integration in the configuration space

$$i\Gamma^{\mu\nu}_{qB\,(A)}(p_1,p_2,p_3) = -ig_s^2 g_f \,\mathbf{tr}\left[t^a t^b\right](2\pi)^8 \left(\frac{4\pi}{qB}\right)^2 \delta^{(2)}\left(p_1 + p_2 - p_3\right)_\perp$$
$$\times \int \frac{d^4 a}{(2\pi)^4}\frac{d^4 b}{(2\pi)^4}\frac{d^4 c}{(2\pi)^4}\delta^{(2)}\left(p_1 + a - c\right)_\parallel \delta^{(2)}\left(p_2 + b - a\right)_\parallel \quad (17)$$
$$\times\, \delta^{(2)}\left(p_3 - c + b\right)_\parallel e^{i\frac{2}{qB}(p_1+a-c)_\mu \hat{F}^{\mu\nu}(p_2+b-a)_\nu}$$
$$\times\, Tr\left[\gamma^\mu S_f^{qB}(a)\gamma^\nu S_f^{qB}(b)S_f^{qB}(c)\right].$$

In order to carry out the integration on the internal momenta, the expressions are generalized to an arbitrary dimension d. Since the presence of the magnetic field separates the parallel and perpendicular components, we will have 2 parallel dimensions and $d-2$ perpendicular dimensions

$$
\begin{aligned}
i\Gamma_{qB\,(A)}^{\mu\nu}(p_1,p_2) = & -ig_s^2 g_f \, \mathbf{tr}\left[t^a t^b\right](2\pi)^4 \left(\frac{4\pi}{qB}\right)^{d-2} \\
& \times \int_0^\infty \frac{ds_1 ds_2 ds_3}{\cos(qBs_1)\cos(qBs_2)\cos(qBs_3)} \\
& \times \int \frac{d^d a}{(2\pi)^d}\frac{d^d b}{(2\pi)^d}\frac{d^d c}{(2\pi)^d} e^{i\frac{2}{qB}(p_1+a-c)\hat{F}(p_2+b-a)} \\
& \times e^{-is_1\left(m^2-a_\parallel^2-a_\perp^2 \frac{\tan(qBs_1)}{qBs_1}\right)} e^{-is_2\left(m^2-b_\parallel^2-b_\perp^2 \frac{\tan(qBs_2)}{qBs_2}\right)} \\
& \times e^{-is_3\left(m^2-c_\parallel^2-c_\perp^2 \frac{\tan(qBs_3)}{qBs_3}\right)} \delta^{(2)}\left(p_1+a-c\right)_\parallel \\
& \times \delta^{(2)}\left(p_2+b-a\right)_\parallel T_{(A)}^{\mu\nu}\left(a_\parallel,a_\perp,b_\parallel,b_\perp,c_\parallel,c_\perp\right).
\end{aligned}
\tag{18}
$$

Hierarchy of scales

Flavor	Electric charge $[e]$	qB_{max} [GeV^2]
Up (u)	2/3	$\sim 10^{-6}$
Down (d)	-1/3	$\sim 4.4 \times 10^{-6}$
Strange (s)	-1/3	$\sim 2 \times 10^{-3}$
Charm (c)	2/3	~ 0.3
Bottom (b)	-1/3	~ 3.5
Top (t)	2/3	$\sim 6 \times 10^3$

Figure: Maximum magnetic field from which the weak field approximation loses validity, it's taken $qB_{max} = 0.2m_f^2$.

For a point of comparison, the maximum field that is created in relativistic heavy ion collisions is

$$eB_{max} \simeq 10m_\pi^2 \sim 2 \times 10^4 \text{ MeV}^2 = 2 \times 10^{-2} \text{ GeV}^2.$$

It is possible to create an homogeneous magnetic field in the z direction with a symmetric gauge

$$A^\mu = \left(0, -\frac{B}{2}x^2, \frac{B}{2}x^1, 0\right). \tag{19}$$

In such a way that the Schwinger phase is

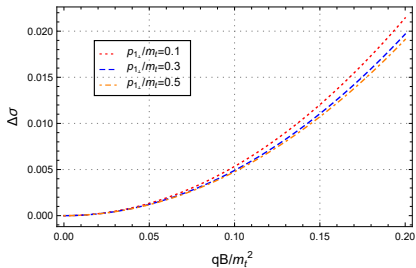$$\Omega_q(x, y) = e^{i\frac{qB}{2}x_\mu \hat{F}^{\mu\nu} y_\nu} = e^{i\frac{qB}{2}\left(x^1 y_2 - x^2 y_1\right)}. \tag{20}$$

Applying (20) to diagrams A and B, the corresponding total phases are

$$\Omega_q(x, y)\Omega_q(y, z)\Omega_q(z, x) = e^{i\frac{qB}{2}\hat{F}^{\mu\nu}\left(x_\mu y_\nu + y_\mu z_\nu + z_\mu x_\nu\right)} = e^{-i\frac{qB}{2}\xi}, \tag{21}$$
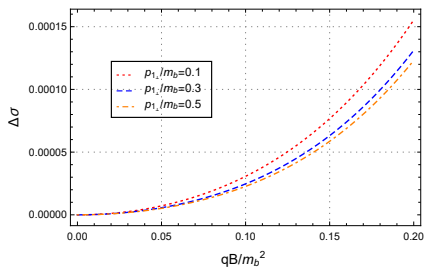
$$\Omega_q(y, x)\Omega_q(z, y)\Omega_q(x, z) = e^{-i\frac{qB}{2}\hat{F}^{\mu\nu}\left(x_\mu y_\nu + y_\mu z_\nu + z_\mu x_\nu\right)} = e^{i\frac{qB}{2}\xi}, \tag{22}$$

where

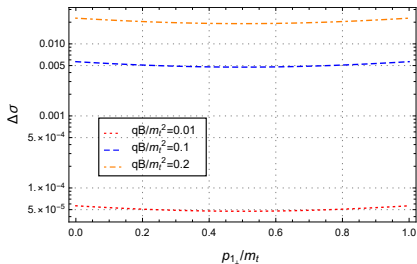$$\xi \equiv -x_2 y^1 + x_1 y^2 - y_2 z^1 + y_1 z^2 - z_2 x^1 + z_1 x^2. \tag{23}$$
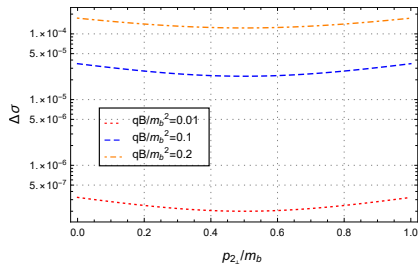
(a) Top quark.

(b) Bottom quark.

Figure: Behavior of the response of the effective section as a function of the magnetic field for the top and bottom quarks, taking different combinations for the values of the transverse moment $p_{1_\perp} + p_{2_\perp} = m_f$ and $\Theta = \pi$.

(a) Top quark.

(b) Bottom quarks.

Figure: Behavior of the response of the cross section as a function of $p_{i_\perp}$ for the top and bottom quarks, taking different values for the magnetic field, $p_{j_\perp} = m_f - p_{i_\perp}$ and $\Theta = \pi$.